arXiv:1603.08899v1 [cond-mat.mtrl-sci] 29 Mar 2016

Thermoelasticity of Fe^{3+}- and Al-bearing bridgmanite

Gaurav Shukla[a,*], Matteo Cococcioni[b], Renata M. Wentzcovitch[a,c]

[a] *School of Physics and Astronomy, University of Minnesota, Minneapolis, Minnesota, USA*
[b] *Theory and Simulation of Materials (THEOS), École polytechnique fédérale de Lausanne, Station 12, CH-1015 Lausanne, Switzerland*
[c] *Department of Chemical Engineering and Materials Science, University of Minnesota, Minneapolis, Minnesota, USA*

Abstract

We report *ab initio* (LDA + U_{sc}) calculations of thermoelastic properties of ferric iron (Fe^{3+})- and aluminum (Al)-bearing bridgmanite ($MgSiO_3$ perovskite), the main Earth forming phase, at relevant pressure and temperature conditions and compositions. Three coupled substitutions, namely, $[Al]_{Mg}$-$[Al]_{Si}$, $[Fe^{3+}]_{Mg}$-$[Fe^{3+}]_{Si}$, and $[Fe^{3+}]_{Mg}$-$[Al]_{Si}$ have been investigated. Aggregate elastic moduli and sound velocities are successfully compared with limited experimental data available. In the case of the $[Fe^{3+}]_{Mg}$-$[Fe^{3+}]_{Si}$ substitution, the high-spin (S=5/2) to low-spin (S=1/2) crossover in $[Fe^{3+}]_{Si}$ induces a volume collapse and elastic anomalies across the transition region. However, the associated anomalies should disappear in the presence of aluminum in the most favorable substitution, i.e., $[Fe^{3+}]_{Mg}$-$[Al]_{Si}$. Calculated elastic properties along a lower mantle model geotherm suggest that the elastic behavior of bridgmanite with simultaneous substitution of Fe_2O_3 and Al_2O_3 in equal proportions or with Al_2O_3 in excess should be similar to that of $(Mg,Fe^{2+})SiO_3$ bridgmanite. Excess Fe_2O_3 should produce elastic anomalies though.

1. Introduction

Aluminum (Al) and iron (Fe)-bearing bridgmanite (br), $(Mg,Fe,Al)(Si,Fe,Al)O_3$ perovskite, is the dominant mineral of the Earth's lower mantle along with (Mg,Fe)O ferropericlase (fp), $CaSiO_3$ perovskite, and $(Mg,Fe,Al)(Si,Fe,Al)O_3$ post-perovskite (PPv). In order to unravel the composition and thermal structure of the lower mantle, a very good estimate of thermal and elastic properties of these constituent minerals is required. In spite of considerable experimental (*Sinnelnikov et al.*, 1998; *Fiquet et al.*, 2000; *Andrault et al.*, 2001; *Jackson et al.*, 2004; *Sinogeikin et al.*, 2004; *Jackson et al.*, 2005b; *Li and Zhang*, 2005; *Murakami et al.*, 2007; *Lundin et al.*, 2008; *Boffa Ballaran et al.*, 2012; *Chantel et al.*, 2012; *Murakami et al.*, 2012; *Dorfman et al.*, 2013) and computational effort (*Karki et al.*, 1999, 2001; *Kiefer et al.*, 2002; *Wentzcovitch et al.*, 2004, 2009; *Wu et al.*, 2009;

*Corresponding author
Email address: shuk0053@umn.edu (Gaurav Shukla)

Wu and Wentzcovitch, 2011; *Tsuchiya and Wang*, 2013; *Wu et al.*, 2013; *Zhang et al.*, 2013; *Wu and Wentzcovitch*, 2014; *Shukla et al.*, 2015a; *Wang et al.*, 2015; *Zhang et al.*, 2016), the available data on high pressure and high temperature elastic properties is still quite limited due to lack of sufficient understanding of the physics and chemistry of these minerals under extreme pressure and temperature conditions typical of the Earth's lower mantle. It has been shown that the iron in (Mg,Fe)O ferropericlase undergoes a pressure induced crossover from a high-spin (S=2) to a low-spin (S=0) state (*Badro et al.*, 2003; *Goncharov et al.*, 2006; *Tsuchiya et al.*, 2006), which noticeably affects elastic properties (*Crowhurst et al.*, 2008; *Marquardt et al.*, 2009; *Wentzcovitch et al.*, 2009; *Wu et al.*, 2009; *Antonangeli et al.*, 2011; *Wu et al.*, 2013; *Wu and Wentzcovitch*, 2014). In the case of Al- and Fe-bearing bridgmanite, the elasticity data base is even more limited due to uncertainties associated with the possible coexistence of ferrous (Fe^{2+}) and ferric (Fe^{3+}) iron and their pressure induced state changes. Moreover, the uncertainties associated with the site occupancy of Al and Fe in the perovskite structure make elasticity measurements and calculations of Al- and Fe-bearing bridgmanite even more challenging. By now it is believed that Fe^{2+} occupies the A-site ($[Fe^{2+}]_{Mg}$), while Fe^{3+} can occupy A- ($[Fe^{3+}]_{Mg}$) and/or B-site ($[Fe^{3+}]_{Si}$) of the perovskite structure (*Badro et al.*, 2004; *Li et al.*, 2004; *Jackson et al.*, 2005a; *Li et al.*, 2006; *Stackhouse et al.*, 2007; *Lin et al.*, 2008; *Bengtson et al.*, 2009; *Dubrovinsky et al.* , 2010; *Hsu et al.*, 2010, 2011; *Fujino et al.*, 2012; *Hummer and Fei*, 2012; *Lin et al.*, 2012, 2013; *Tsuchiya and Wang*, 2013; *Caracas et al.*, 2014; *Sinmyo et al.*, 2014; *Mao et al.*, 2015). In the entire lower mantle pressure-range, $[Fe^{2+}]_{Mg}$ remains in the HS state (S=2) but undergoes a pressure induced lateral displacement (*Bengtson et al.*, 2009; *Hsu et al.*, 2010), which results in a state with increased iron Mössbauer quadrupole splitting (QS) (*McCammon et al.*, 2008; *Bengtson et al.*, 2009; *Hsu et al.*, 2010; *Lin et al.*, 2012, 2013; *McCammon et al.*, 2013; *Potapkin et al.*, 2013; *Kupenko et al.*, 2014; *Shukla et al.*, 2015a). On the other hand, $[Fe^{3+}]_{Si}$ goes from the HS (S=5/2) to the LS (S=1/2) state and $[Fe^{3+}]_{Mg}$ remains in the HS (S=5/2) state throughout the lower mantle pressure region (*Catalli et al.*, 2010, 2011; *Fujino et al.*, 2012, 2014; *Hsu et al.*, 2011; *Lin et al.*, 2012, 2013; *Tsuchiya and Wang*, 2013; *Mao et al.*, 2015; *Shukla et al.*, 2015b; *Xu et al.*, 2015). For Al-bearing bridgmanite, experimental observations suggest that Al enters the lattice through coupled substitutions as $[Al]_{Mg}$-$[Al]_{Si}$ (*Andrault et al.*, 2001; *Jackson et al.*, 2004, 2005b). In the case of simultaneous substitution of Al and Fe^{3+} in bridgmanite, *Hsu et al.* (2012) reported that $[Fe^{3+}]_{Mg}$-$[Al]_{Si}$ substitution is energetically favored with $[Fe^{3+}]_{Mg}$ remaining in the HS state (S=5/2) in the entire lower mantle pressure range.

Based on X-ray emission spectroscopy (XES) and Synchrotron Mössbauer spectroscopy (SMS), it has been suggested that $[Fe^{3+}]_{Si}$ in Fe^{3+}-bearing bridgmanite undergoes a pressure induced HS to LS crossover in the pressure range 48-63 GPa (*Catalli et al.*, 2010) and 18-25 GPa (*Lin et al.*, 2012; *Mao et al.*, 2015) for the samples containing ~10 mol.% and ~0.01 mol.% Fe_2O_3, respectively. Using Synchrotron X-ray diffraction data, *Mao et al.* (2015) recently observed a noticeable volume collapse across the crossover region and this observation is consistent with the previous *ab initio* predictions (*Hsu et al.*, 2011; *Tsuchiya and Wang*, 2013). Similarly to the spin crossover in (MgFe)O ferropericlase (*Jackson et al.*, 2006; *Crowhurst et al.*,

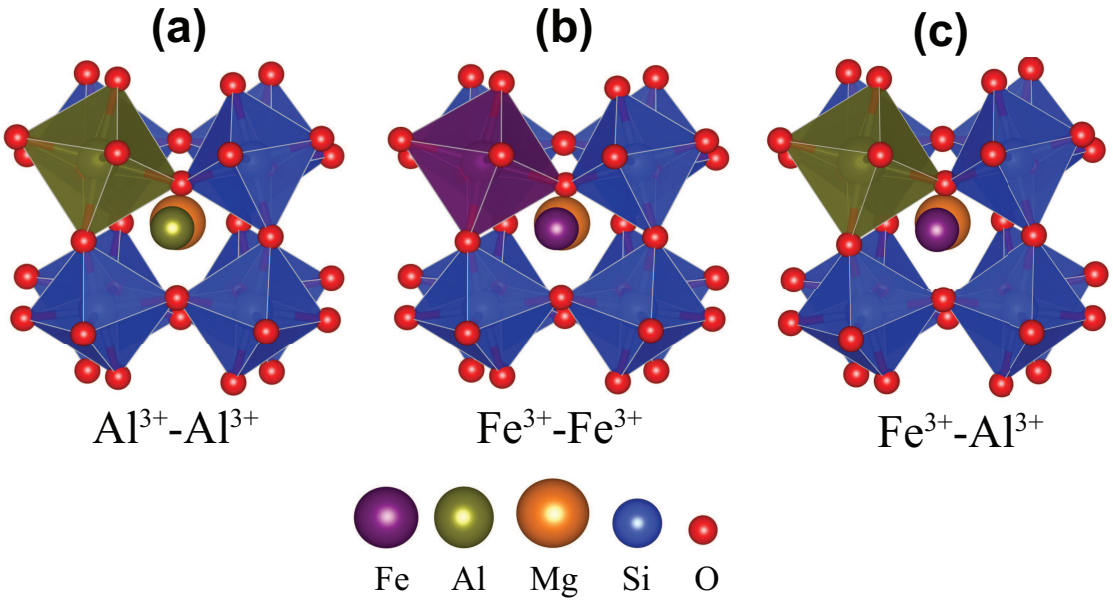

Figure 1: (a) Atomic structure of Al- and Fe^{3+}-bearing bridgmanite with coupled substitutions (a) $[Al]_{Mg}$-$[Al]_{Si}$, (b) $[Fe^{3+}]_{Mg}$-$[Fe^{3+}]_{Si}$, and (c) $[Fe^{3+}]_{Mg}$-$[Al]_{Si}$. Fe,Al, Mg, Si, and O are represented as purple, green, orange, blue, and red sphere, respectively.

2008; *Marquardt et al.*, 2009; *Antonangeli et al.*, 2011; *Wentzcovitch et al.*, 2009; *Wu et al.*, 2009, 2013), this volume collapse should cause elastic anomalies across the spin crossover region. These anomalies may have significant impact on the lower mantle properties (*Wu and Wentzcovitch*, 2014). Owing to extremely high pressure and temperature conditions, experimental observations of elastic anomalies of Fe^{3+}-bearing bridgmanite are still not available. Using *ab initio* molecular dynamics (MD) simulations, *Zhang et al.* (2016) recently calculated thermoelastic properties of $[Fe^{3+}]_{Mg}$-$[Al]_{Si}$-bearing bridgmanite. Their calculations were limited to few pressures and temperatures, did not include effect of strong correlation on Fe^{3+}, and conclusions about lower mantle composition were fitting parameters dependent. They also did not consider the effect of iron spin crossover on elastic properties. Here we present an *ab initio* quasiharmonic calculation of thermoelastic properties of Al- and Fe^{3+}-bearing bridgmanite. This should help to clarify the potential consequences of the spin crossover of $[Fe^{3+}]_{Si}$ for lower mantle properties.

2. Computational details

Here we have used density functional theory augmented by the self- and structurally consistent Hubbard type correction (DFT + U_{sc} method)(*Cococcioni and de Gironcoli*, 2005; *Kulik et al.*, 2006) within the local density approximation (LDA) (*Ceperley and Alder*, 1980) to address the strong Coulomb correlation effects among iron 3*d* electrons. Three cou-

pled substitutions of Al and Fe^{3+} (shown in Figure 1): $(Mg_{1-x}Al_x)(Si_{1-x}Al_x)O_3$ (Al-br), $(Mg_{1-x}Fe_x)(Si_{1-x}Fe_x)O_3$ (Fe^{3+}-br), and $(Mg_{1-x}Fe_x)(Si_{1-x}Al_x)O_3$ bridgmanite (Fe^{3+}-Al-br) for $x = 0.125$ have been investigated. U_{sc} values used here have been reported previously by *Hsu et al.* (2011). Elastic moduli and density for $0 < x < 0.125$ have been linearly interpolated using calculated results for $x = 0$ and $x = 0.125$. All calculations have been performed in a 40-atom super-cell ($x = 0.125$). Ultra-soft pseudo-potentials (*Vanderbilt*, 1990) have been used for Al, Fe, Si, and O. For Mg, a norm-conserving pseudo-potential generated by von Barth-Car's method has been used. A detailed description of these pseudo-potentials has been reported by *Umemoto et al.* (2008). The plane-wave kinetic energy and charge density cut-off are 40 Ry and 160 Ry, respectively. For all three configurations mentioned above, the electronic states have been sampled on a shifted $2\times2\times2$ k-point grid (*Monkhorst and Pack*, 1976). The equilibrium geometry at arbitrary pressure has been obtained using the variable cell-shape damped molecular dynamics (VCS-MD) (*Wentzcovitch*, 1991; *Wentzcovitch et al.*, 1993). Vibrational effects have been addressed within the quasiharmonic approximation (QHA) (*Carrier et al.*, 2007; *Wallace*, 1972). Vibrational density of states (VDOS) have been computed using the density functional perturbation theory (DFPT) (*Baroni et al.*, 2001) within the LDA + U_{sc} implementation (*Floris et al.*, 2011) for the exchange-correlation energy functional.

Aggregate elastic moduli and acoustic velocities were calculated for $[Al]_{Mg}$-$[Al]_{Si}$, $[Fe^{3+}]_{Mg}$-$[Fe^{3+}]_{Si}$, and $[Fe^{3+}]_{Mg}$-$[Al]_{Si}$ substitutions using a semi-analytical method (SAM) (*Wu and Wentzcovitch*, 2011). For this purpose, equilibrium structures were obtained at 10-12 pressure points in the relevant pressure-range and dynamical matrices at each pressure point were calculated using DFPT in a $2 \times 2 \times 2$ q-point grid. Thus, obtained force constants from dynamical matrices were interpolated in a $8 \times 8 \times 8$ q-point grid to obtain VDOS. The static elastic coefficients, C_{ijkl}^{static}, were obtained at each pressure by applying small $\pm1\%$ strains to the equilibrium structure, relaxing internal degrees of freedom, computing internal stresses and extracting them from the stress-strain relation $\sigma_{ij} = \sum C_{ijkl}\epsilon_{kl}$. This strain is small enough to maintain linearity in the stress-strain relation and large enough for good numerical accuracy in the calculation. Owing to the orthorhombic crystal symmetry, bridgmanite has nine independent elastic constants (i.e., C_{11}, C_{22}, C_{33}, C_{44}, C_{55}, C_{66}, C_{12}, C_{13}, C_{23} in Voigt notation). Bulk (K) and shear modulus (G) have been estimated by computing Voigt-Reuss-Hill averages (*Watt et al.*, 1976). Using K and G along with the high temperature equation of states (for density, ρ), we obtained the pressure and temperature dependent acoustic velocities (compressional velocity, $V_P = \sqrt{\frac{K+\frac{4}{3}G}{\rho}}$, shear velocity, $V_S = \sqrt{\frac{G}{\rho}}$, and bulk velocity, $V_\Phi = \sqrt{\frac{K}{\rho}}$).

3. Results and discussion

3.1. Elasticity of $[Al]_{Mg}$-$[Al]_{Si}$-bearing bridgmanite

Our calculated aggregate elastic moduli (K and G), acoustic velocities (V_P, V_S, and V_Φ), and density for pure $MgSiO_3$ and Al-bearing bridgmanite are shown in Figure 2. Results of pure $MgSiO_3$ shown here have been taken from our previous study (*Shukla et al.*, 2015a). Our calculated high temperature results, especially shear moduli and shear velocities at 2700 K, are

in good agreement with experimental data (*Li and Zhang*, 2005; *Chantel et al.*, 2012; *Murakami et al.*, 2012) (Figure 2a and 2a′), which shows that *ab initio* methods used here provide a robust estimate for elastic properties of minerals at pressure and temperature conditions typical of the Earth's lower mantle. Our results for Al-br with $x = 0.05$ at 300 K also compare well with the room temperature data by *Jackson et al.* (2005b) and *Murakami et al.* (2012) for Al-bearing samples containing ~5 wt% and ~4 wt% of Al_2O_3, respectively (Figure 2b and 2b′). For Al-br, calculated pressure derivatives of elastic moduli, K' and G', are 4.06 and 1.85, respectively. These values are fairly comparable with those reported by *Jackson et al.* (2005b) (Table 1). In overall, our results of Al_2O_3 substitution at 300 K are consistent with previous experimental studies (*Jackson et al.*, 2004, 2005b; *Murakami et al.*, 2012).

3.2. Elasticity of $[Fe^{3+}]_{Mg}$-$[Fe^{3+}]_{Si}$ and $[Fe^{3+}]_{Mg}$-$[Al]_{Si}$-bearing bridgmanite

Having successfully calculated the elastic properties for pure and Al-bearing bridgmanite, we now investigate the elastic consequences of the pressure induced spin crossover of $[Fe^{3+}]_{Si}$ in $(Mg_{1-x}Fe_x)(Si_{1-x}Fe_x)O_3$ bridgmanite (Fe^{3+}-br). For this purpose, we calculate elastic properties of the system in the mixed spin state (MS) by extending the approach developed by *Wu et al.* (2013). The elastic compliances S^{ij} of Fe^{3+}-br in the MS state are given by (see Supporting Information for details)

$$S^{ij}V = nS^{ij}_{LS}V_{LS} + (1-n)S^{ij}_{HS}V_{HS} - \frac{1}{9}(V_{LS} - V_{HS})\frac{\partial n}{\partial P} \tag{1}$$

for $i, j = 1-3$ and

$$S^{ii}V = nS^{ii}_{LS}V_{LS} + (1-n)S^{ii}_{HS}V_{HS} \tag{2}$$

for $i = 4-6$. Here $S^{ij}_{HS/LS}$ and $V_{HS/LS}$ are the elastic compliances and volume of pure HS/LS state, respectively. n is the low-spin (LS) fraction of $[Fe^{3+}]_{Si}$ and is given by

$$n(P,T) = \frac{1}{1 + \frac{m_{HS}(2S_{HS}+1)}{m_{LS}(2S_{LS}+1)}\exp\left\{\frac{\Delta G_{LS\rightarrow HS}}{xk_BT}\right\}}, \tag{3}$$

where $S_{HS/LS}$ is spin moment ($S_{HS} = 5/2$, $S_{LS} = 1/2$), $m_{HS/LS}$ is the orbital degeneracy ($m_{HS} = 1$, $m_{LS} = 3$) of HS/LS state, k_B is the Boltzmann constant, and $\Delta G_{LS\rightarrow HS} = G^{stat+vib}_{LS} - G^{stat+vib}_{HS}$. Elastic coefficients C_{ij} are obtained using the relation: $\mathbf{C}_{ij} = \left[\mathbf{S}^{-1}\right]^{ij}$

The pressure and temperature dependence of LS fraction of $[Fe^{3+}]_{Si}$, $n(P,T)$, in Fe^{3+}-br for $x = 0.125$ is shown in Figure 3a. The spin crossover pressure range in our calculation is much broader than that reported by *Tsuchiya and Wang* (2013). Our estimated transition pressure width at 300 K is about ~8 GPa, in fairly good agreement with the experimental data (*Catalli et al.*, 2010; *Lin et al.*, 2012; *Mao et al.*, 2015), while the one reported by *Tsuchiya and Wang* (2013) is <2 GPa. This difference may be related to the use of different values of Hubbard U and different technique for VDOS calculations. The values of U used

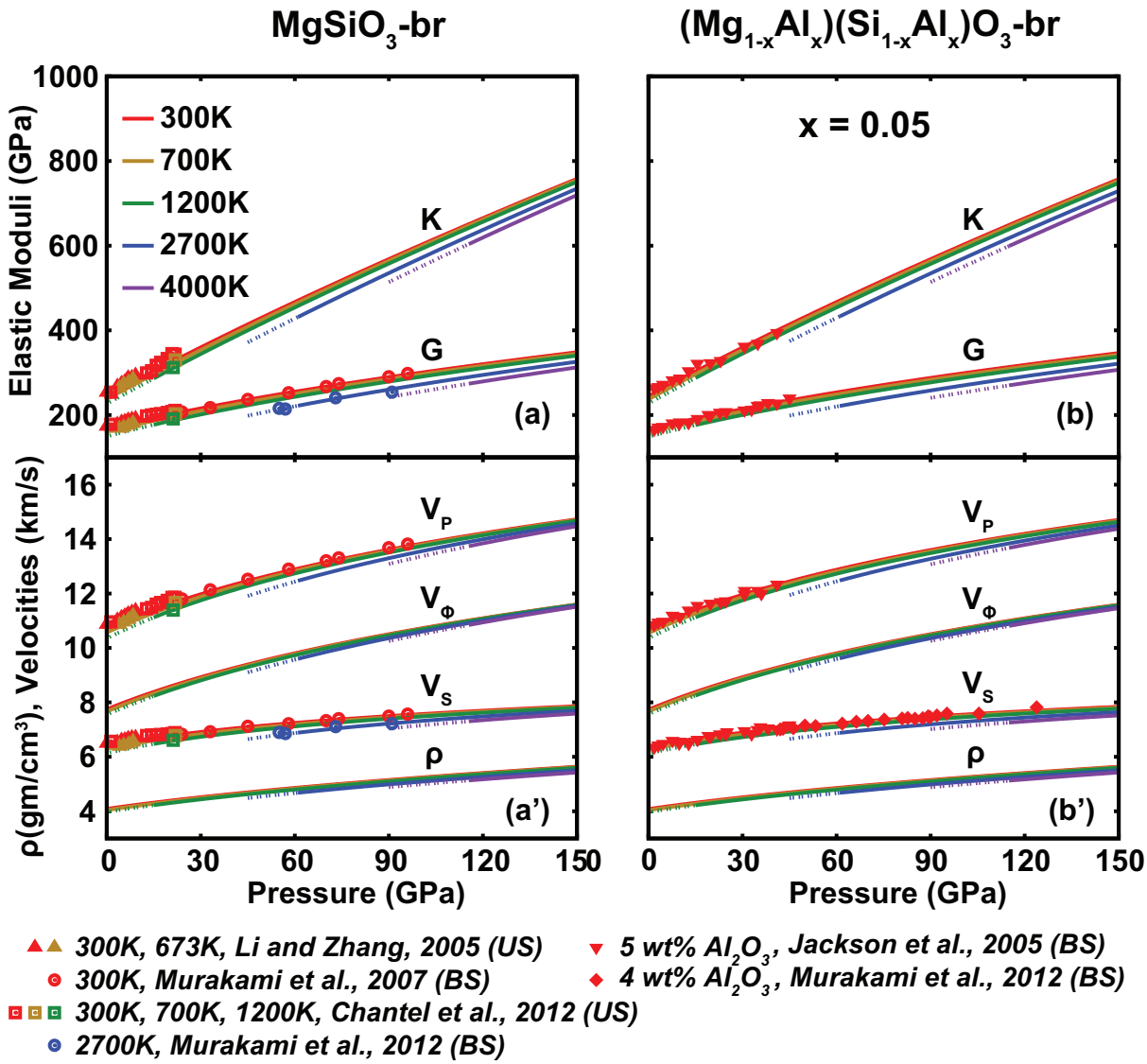

Figure 2: Pressure and temperature dependence of elastic moduli, acoustic velocities, and density for (a,a') pure $MgSiO_3$ and (b,b') $(Mg_{0.95}Al_{0.05})(Si_{0.95}Al_{0.05})O_3$ bridgmanite. Results for pure $MgSiO_3$ are taken from our previous study (*Shukla et al.*, 2015a). Our calculated results (lines) are compared with available experimental data (symbols). Solid (dashed) lines represent *ab initio* results within (outside) the validity of quasi-harmonic approximation. BS: Brillouin scattering, US: ultrasonic technique.

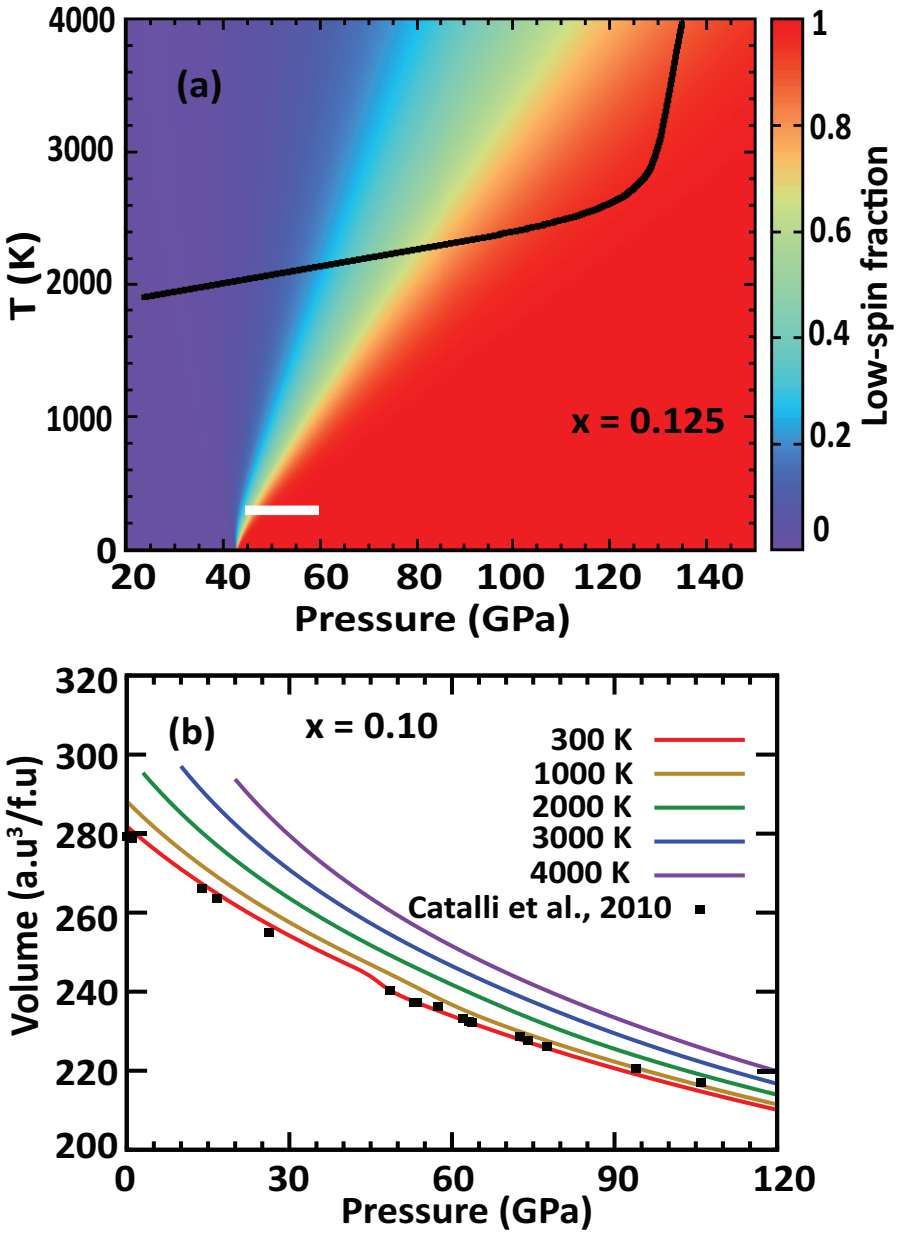

Figure 3: (a) Pressure and temperature dependence of low-spin fraction, n(P,T), of $[Fe^{3+}]_{Si}$ in $(Mg_{1-x}Fe^{3+}_x)(Si_{1-x}Fe^{3+}_x)O_3$ bridgmanite for $x = 0.125$. Solid black curve represents the lower mantle model geotherm by (*Boehler*, 2000), while white bar represents the experimental pressure range at room temperature in which spin crossover of $[Fe^{3+}]_{Si}$ is complete (*Catalli et al.*, 2010). (b) Pressure dependence of calculated volume at several temperature for $x = 0.10$. Compression curve at 300 K (red) is compared with experimental data by *Catalli et al.* (2010) (black squares).

Table 1: Calculated volume (V), elastic moduli (K, G), their pressure derivatives (K', G'), and acoustic velocities (V_P, V_S, V_Φ) for Al- and Fe-bearing bridgmanite (br) at 0 GPa and 300 K. [a] See Table 1 in *Shukla et al.* (2015a) for detailed comparison of br and Fe^{2+}-br results with experimental data

	$V(Å^3)$	K (GPa)	G (GPa)	K'	G'	V_P	V_S	V_Φ	References
br ($x = 0$)[a]	163.2	245.5	168.2	3.96	1.79	10.72	6.42	7.74	*Shukla et al.* (2015a)
Fe^{2+}-br ($x = 0.125$)[a]	163.7	246.7	165.2	4.03	1.80	10.50	6.25	7.64	*Shukla et al.* (2015a)
Al-br ($x = 0.125$)	164.1	242.5	162.7	4.06	1.85	10.62	6.32	7.72	*This study*
Al-br ($x \approx 0.0.5$)	163.26(1)	252(5)	165(2)	3.7(0.3)	1.7(0.2)	10.75(5)	6.35(5)	7.85(5)	*Jackson et al.* (2004, 2005b)
Fe^{3+}-br ($x = 0.125$)	168.0	233.6	143.1	4.05	1.88	9.98	5.80	7.40	*This study*
Fe^{3+}-Al-br ($x = 0.125$)	165.3	239.4	156.3	4.05	1.83	10.34	6.11	7.56	*This study*

here were calculated self-consistently, while those reported by *Tsuchiya and Wang* (2013) were not. *Tsuchiya and Wang* (2013) used the finite displacement method (*Alfè*, 2009) to calculate the VDOS. This method disregards the calculation of dielectric constant tensor that leads to LO-TO splitting for polar materials. In this work, we have used DFPT + U method developed by *Floris et al.* (2011) for computing dynamical matrices and phonon frequencies. This method has been successfully used to address vibrational properties and the $[Fe^{2+}]_{Mg}$ displacement transition in Fe^{2+}-bearing bridgmanite (*Shukla et al.*, 2015a). Our calculated 300 K compression curve for Fe^{3+}-br with $x = 0.10$ also compare well with experimental data (*Catalli et al.*, 2010) (Figure 3b). Therefore, we believe that calculation of VDOS and its free-energy contribution using DFPT + U method is quite robust.

Our results for elastic moduli, acoustic velocities, and density of Fe^{3+}-br with $x = 0.05$ are shown in Figure 4a and 4a′. The spin crossover of $[Fe^{3+}]_{Si}$ produces anomalous softening in the bulk modulus in the crossover pressure region and this anomalous behavior is also reflected in compressional (V_P) and bulk velocities (V_Φ). The strength of the anomaly depends on temperature, volume difference ($\Delta V_{HS\rightarrow LS} = V_{LS} - V_{HS}$), and Gibb's free energy difference ($\Delta G_{HS\rightarrow LS} = G_{LS} - G_{HS}$). $\Delta V_{HS\rightarrow LS}$ for Fe^{3+}-br with $x = 0.01$ is approximately ∼-0.15% (Figure 3b), which is in good agreement with previous *ab initio* calculations (*Hsu et al.*, 2011; *Tsuchiya and Wang*, 2013) and is fairly comparable to experimental value ∼-0.2% (*Mao et al.*, 2015). This volume reduction causes quite a significant softening in the bulk modulus (∼12% at 300 K), while the shear modulus increases only by a small amount (∼0.5% at 300 K) across the transition region.

Effects of Al substitution on the spin crossover of Fe^{3+} was previously studied by *Hsu et al.* (2012) using *ab initio* static calculations within the LDA + U_{sc} approximation. The coupled substitution $[Fe^{3+}]_{Mg}$-$[Al]_{Si}$ was found to be energetically favorable. Therefore, we have chosen this substitution to investigate the elastic properties of bridgmanite due to simultaneous inclusion of Al and Fe. Elastic moduli and acoustic velocities for $(Mg_{1-x}Fe_x)(Si_{1-x}Al_x)O_3$ bridgmanite with $x = 0.10$ are shown in Figure 4b and Figure 4b′. $[Fe^{3+}]_{Mg}$ is in the HS (S = 5/2) state in the entire lower mantle pressure range. Owing to the absence of any spin state crossover in $[Fe^{3+}]_{Mg}$-$[Al]_{Si}$ substitution, the elastic anomalies, otherwise present in the Fe^{3+}-bearing bridgmanite, disappear in this case.

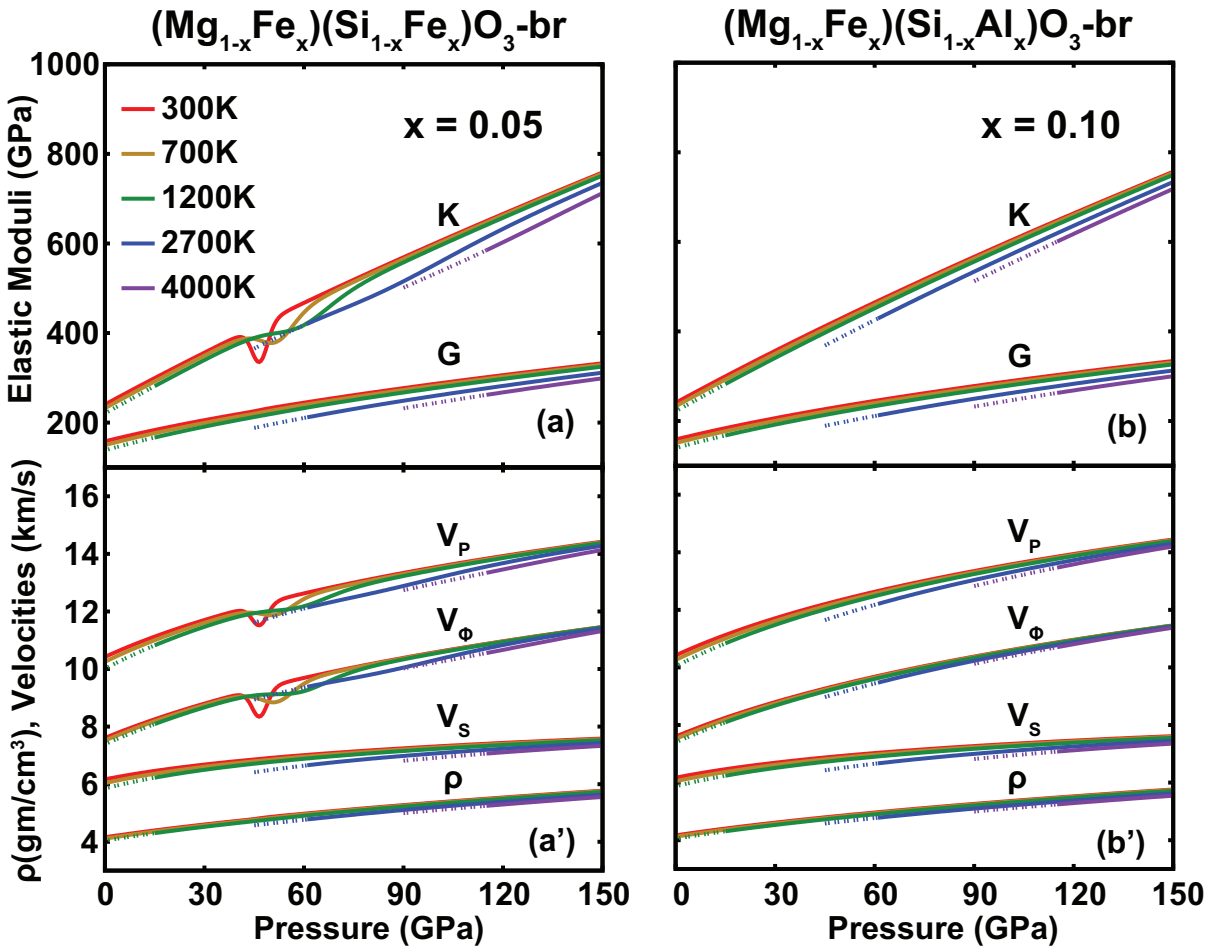

Figure 4: Pressure and temperature dependence of elastic moduli (bulk modulus K, and shear modulus G) and acoustic velocities (compressional velocity V_P, shear velocity V_S, and bulk velocity V_Φ) for (a,a') $(Mg_{0.95}Fe_{0.05})(Si_{0.95}Fe_{0.05})O_3$ and (b,b') $(Mg_{0.90}Fe_{0.10})(Si_{0.90}Al_{0.10})O_3$ bridgmanite. Solid (dashed) lines represent *ab initio* results within (outside) the validity of quasi-harmonic approximation.

4. Geophysical significance

Understanding the effect of Al and Fe substitution on the elastic properties of bridgmanite is essential to unravel the composition, thermal structure, nature of seismic heterogeneities, and dynamics of the Earth's lower mantle. Table 1 compares calculated volume, elastic moduli (bulk modulus, K, and shear modulus, G), their pressure derivatives (K′, G′), and acoustic velocities (V_P, V_S, and V_Φ) at ambient pressure and temperature conditions for the most relevant substitutions. Inclusion of 12.5 mol.% of Al_2O_3 in bridgmanite changes volume, K, and G by ∼0.5%, ∼ −1.2%, and ∼ −3.5%, respectively. This trend becomes more noticeable when the same amount (12.5 mol.%) of Fe_2O_3 is substituted, which results in ∼3%, ∼ −5%, and ∼ −15% change in volume, K, and G, respectively. It is important to note that the effect of Fe_2O_3 substitution is different from that of FeO. As seen in Table 1, the presence of 12.5 mol.% of FeO increases K by ∼0.5%, while the same amount of Fe_2O_3 decreases it by ∼5%. Simultaneous substitution of Fe_2O_3 and Al_2O_3 as $[Fe^{3+}]_{Mg}$-$[Al]_{Si}$ changes the volume, K, and G by ∼1.3%, ∼ −2.5%, and ∼ −7%, respectively. These changes in volume and elastic moduli due to Al and Fe substitutions are also reflected in acoustic velocities. The incorporation of 12.5 mol.% of Al_2O_3 in bridgmanite, changes V_P, V_S, and V_Φ by ∼ −0.9%, ∼ −1.6%, and ∼ −0.3%, respectively, while the same amount of Fe_2O_3 changes these values by ∼ −6.9%, ∼ −9.7%, and ∼ −4.4%, respectively. For simultaneous substitution of Al_2O_3 and Fe_2O_3, the change in V_P, V_S, and V_Φ is ∼ −3.5%, ∼ −4.8%, and ∼ −2.3%, respectively.

Table 2 compares $\frac{dK}{dT}$ and $\frac{dG}{dT}$ for various Fe and Al substitutions at 300 K and 0, 60, and 120 GPa. Results for pure, Fe^{2+}-, and $[Fe^{3+}]_{Mg}$-$[Al]_{Si}$-bearing bridgmanite are very similar. This observation suggests that the temperature dependence of elastic properties due to simultaneous inclusion of Al_2O_3 and Fe_2O_3 in bridgmanite would be nearly indistinguishable from those of FeO substitution with the same amount of iron.

Figure 5 shows calculated elastic moduli, acoustic velocities, and density along a model lower mantle geotherm (*Boehler*, 2000) for $(Mg_{0.95}Al^{3+}_{0.05})(Si_{0.95}Al^{3+}_{0.05})O_3$, $(Mg_{0.95}Fe^{3+}_{0.05})(Si_{0.95}Fe^{3+}_{0.05})O_3$, $(Mg_{0.90}Fe^{3+}_{0.10})(Si_{0.90}Al^{3+}_{0.10})O_3$, and $(Mg_{0.90}Fe^{2+}_{0.10})SiO_3$ bridgmanite. These concentrations were chosen to represent the expected composition of bridgmanite in the lower mantle (*Irifune et al.*, 2010). Results are also compared with those of pure $MgSiO_3$ and with Preliminary Reference Earth Model (PREM) (*Dziewonski and Anderson*, 1981). The inclusion of Al_2O_3 does not seem to affect the elastic properties of bridgmanite significantly (Figure 5a and 5a′). The anomalous softening due to spin crossover of $[Fe^{3+}]_{Si}$ is present in the $[Fe^{3+}]_{Mg}$-$[Fe^{3+}]_{Si}$ substitution (Figure 5b and 5b′). However, these anomalies no longer exist with the simultaneous substitutions of Al and Fe as $[Fe^{3+}]_{Mg}$-$[Al]_{Si}$. This substitution mechanism, its elastic properties, and the likely low concentration of Fe^{3+} in br (*Xu et al.*, 2015), might explain the lack of sizeable spin crossover induced elastic anomalies in the PREM model (*Dziewonski and Anderson*, 1981). In addition, the elastic properties of $(Mg_{0.90}Fe^{3+}_{0.10})(Si_{0.90}Al^{3+}_{0.10})O_3$ are very similar to those of $(Mg_{0.90}Fe^{2+}_{0.10})SiO_3$ bridgmanite or to PREM velocities, except for the bulk modulus, K, and compressional velocity, V_P. Relatively larger K and V_P

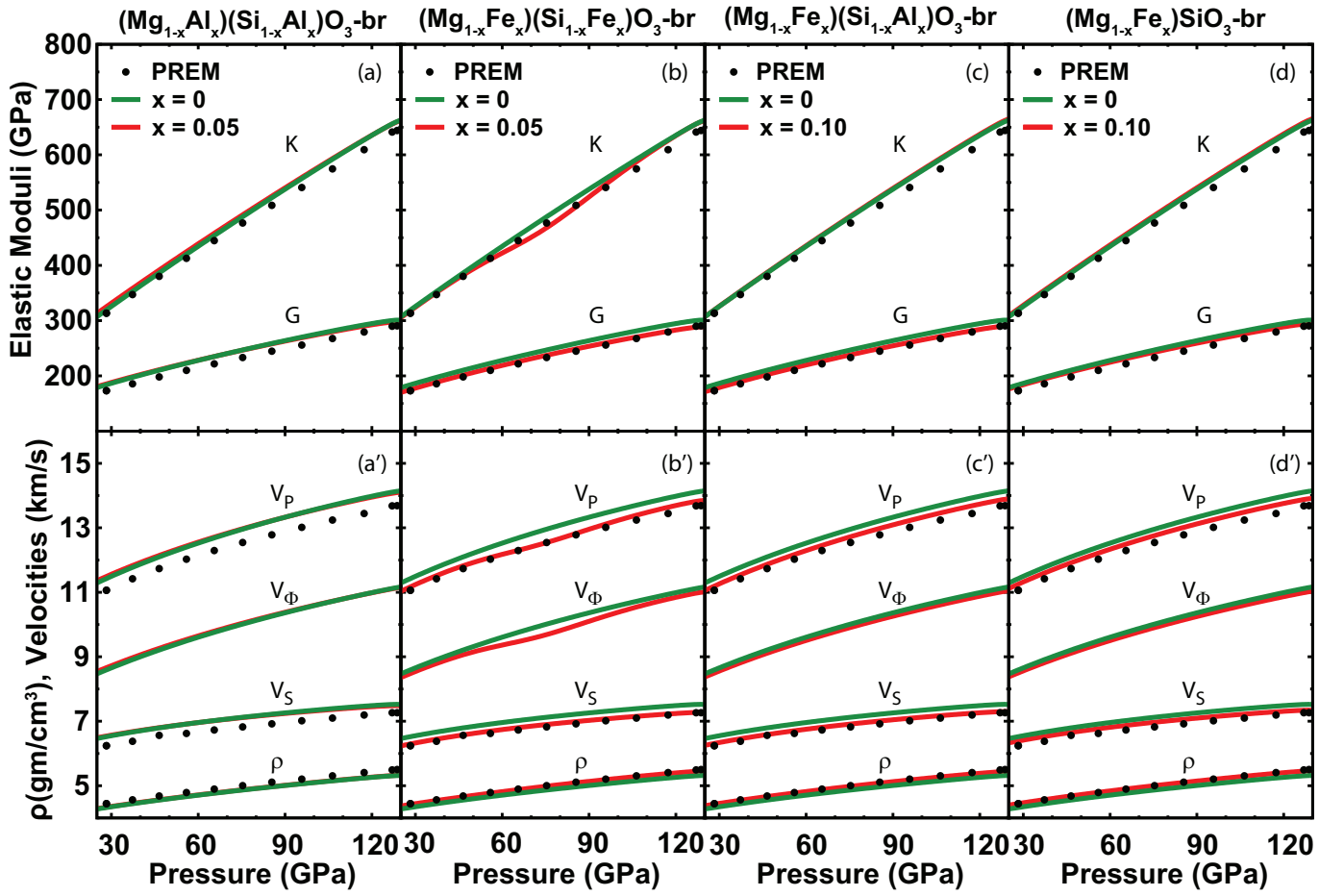

Figure 5: Elastic moduli, acoustic velocities, and density along a model lower mantle geotherm by *Boehler, 2000* (*Boehler*, 2000) for (a,a') $[Al]_{Mg}$-$[Al]_{Si}$, (b,b') $[Fe^{3+}]_{Mg}$-$[Fe^{3+}]_{Si}$, (c,c') $[Fe^{3+}]_{Mg}$-$[Al]_{Si}$, and $[Fe^{2+}]_{Mg}$ substitution in $MgSiO_3$ bridgmanite. Calculated results (red lines) are compared with that of pure $MgSiO_3$ bridgmanite (green lines) and with the Preliminary Reference Earth Model (PREM) (*Dziewonski and Anderson*, 1981) data (black points).

Table 2: Calculated temperature derivatives of aggregate elastic moduli in unit of GPa/K at 300 K and 0, 60, and 120 GPa.

	$\frac{dK(0,300)}{dT}$	$\frac{dK(60,300)}{dT}$	$\frac{dK(120,300)}{dT}$	$\frac{dG(0,300)}{dT}$	$\frac{dG(60,300)}{dT}$	$\frac{dG(120,300)}{dT}$
br ($x = 0$)	-0.0157	-0.0093	-0.0054	-0.0178	-0.0108	-0.0077
Fe^{2+}-br ($x = 0.125$)	-0.0160	-0.0097	-0.0059	-0.0178	-0.0107	-0.0077
Al-br ($x = 0.125$)	-0.0116	-0.0095	-0.0086	-0.0144	-0.0109	-0.0095
Fe^{3+}-br ($x = 0.125$)	-0.0191	-0.0088	-0.0001	-0.0205	-0.0101	-0.0066
Fe^{3+}-Al-br ($x = 0.125$)	-0.0165	-0.0097	-0.0054	-0.0182	-0.0106	-0.0074

compared to PREM values suggest that the lower mantle may accommodate a reasonable amount of ferropericlase, (MgFe)O, and $CaSiO_3$ perovskite, consistent with conclusions of previous first principles calculations (*Wentzcovitch et al.*, 2004).

5. Conclusions

We have presented *ab initio* calculations of thermoelastic properties Al- and Fe^{3+}-bearing bridgmanite. Aggregate elastic moduli, acoustic velocities, and density for three coupled substitutions, $[Al]_{Mg}$-$[Al]_{Si}$, $[Fe^{3+}]_{Mg}$-$[Fe^{3+}]_{Si}$, and $[Fe^{3+}]_{Mg}$-$[Al]_{Si}$ have been computed by combining the vibrational density of states and static LDA/LDA + U_{sc} calculations within the quasi-harmonic approximation. Results for pure $MgSiO_3$ and Al-bearing bridgmanite compare very well with available experimental data (*Li and Zhang*, 2005; *Jackson et al.*, 2005b; *Chantel et al.*, 2012; *Murakami et al.*, 2007, 2012). Elastic anomalies due to spin crossover of $[Fe^{3+}]_{Si}$ in Fe^{3+}-bearing bridgmanite cease to exist in the presence of Al_2O_3. Elastic properties calculated along a model lower mantle geotherm (*Boehler*, 2000) suggest that Al_2O_3 may be accommodated with Fe_2O_3 in a coupled substitution without altering the overall elastic properties of $(Mg,Fe^{2+})SiO_3$ bridgmanite.

Appendix A. Solid solution model for elasticity of mixed spin state (MS) of HS and LS state of $[Fe^{3+}]_{Si}$ in Fe^{3+}-bearing bridgmanite

The molar Gibb's free energy for the system (under stress σ) in the MS state is given by

$$G(P,T,n,\sigma) = nG_{LS}(P,T,\sigma) + (1-n)G_{HS}(P,T,\sigma) + G^{mix}(P,T,\sigma), \tag{A.1}$$

where $n(P,T,\sigma)$ is the low-spin (LS) fraction, T is temperature, P is pressure, $G_{LS/HS}$ is the Gibb's free energy for pure HS/LS state. G^{mix} is the mixing free energy for ideal solid solution of HS and LS states of $[Fe^{3+}]_{Si}$ and is given by

$$G^{mix}(P,T) = xk_BT[nln(n) + (1-n)ln(1-n)], \tag{A.2}$$

where x is Fe_2O_3 molar concentration, k_B is Boltzmann constant.

The Gibb's free energy for pure HS/LS state is given as

$$G_{HS/LS}(T,V) \quad = \quad G^{stat+vib}_{HS/LS}(T,V) + G^{mag}_{HS/LS}(T,V), \tag{A.3}$$

where $G^{stat+vib}_{HS/LS}(T,V)$ is the internal energy (obtained from 'static' calculation) and vibrational contribution Gibb's free-energy. $G^{mag}_{HS/LS}(T,V)$ is the magnetic contribution to free-energy, which is given by

$$\begin{aligned} G^{mag}_{HS}(T,V) &= -xk_BTln\left[m_{HS}(S_{HS}+1)\times m_{HS}(S_{HS}+1)\right], and \\ G^{mag}_{HS}(T,V) &= -xk_BTln\left[m_{HS}(S_{HS}+1)\times m_{LS}(S_{LS}+1)\right], \end{aligned} \tag{A.4}$$

where $S_{HS/LS}$ is spin (S_{HS} = 5/2, S_{LS} = 1/2) and $m_{HS/LS}$ is orbital degeneracy (m_{HS} = 1, m_{LS} = 3) of HS/LS state of $[Fe^{3+}]_{Si}$.

Minimizing $G(P,T,n,\sigma)$ (Eq. A.1) with respect to LS fraction $n(P,T,\sigma)$, we obtain

$$n(P,T,\sigma) = \frac{1}{1+\frac{m_{HS}(2S_{HS}+1)}{m_{LS}(2S_{LS}+1)}\exp\left\{\frac{\Delta G_{LS\rightarrow HS}}{xk_BT}\right\}}, \tag{A.5}$$

where $\Delta G_{LS\rightarrow HS} = G^{stat+vib}_{LS} - G^{stat+vib}_{HS}$.

The elastic compliances S^{ij} of the system in MS state are calculated as

$$S^{ij} = -\frac{1}{V}\frac{\partial^2 G}{\partial\sigma_i\partial\sigma_j}\bigg|_{P,T}. \tag{A.6}$$

The derivative of G with respect to σ is computed from Eq. (A.1)

$$\frac{\partial G}{\partial\sigma_i} = n\frac{\partial G_{LS}}{\partial\sigma_i} + (1-n)\frac{\partial G_{HS}}{\partial\sigma_i} + (G_{LS}-G_{HS})\frac{\partial n}{\partial\sigma_i} + \frac{\partial G^{mix}}{\partial\sigma_i}. \tag{A.7}$$

However, at equilibrium

$$\frac{\partial G}{\partial n} = \left[(G_{LS}-G_{HS})\frac{\partial n}{\partial\sigma_i} + \frac{\partial G^{mix}}{\partial\sigma_i}\right]\frac{\partial\sigma_i}{\partial n} = 0. \tag{A.8}$$

In Eq. (A.8), the derivative $\frac{\partial\sigma_i}{\partial n} \neq 0$ ensures that

$$(G_{LS}-G_{HS})\frac{\partial n}{\partial\sigma_i} + \frac{\partial G^{mix}}{\partial\sigma_i} = 0. \tag{A.9}$$

Therefore, the elastic compliances for the system in MS state are

$$S^{ij}V = nS^{ij}_{LS}V_{LS} + (1-n)S^{ij}_{HS}V_{HS} + \left(\frac{\partial G_{HS}}{\partial\sigma_i} - \frac{\partial G_{LS}}{\partial\sigma_i}\right)\frac{\partial n}{\partial\sigma_j}, \tag{A.10}$$

where volume V in MS state is calculated using $V = nV_{LS} + (1-n)V_{HS}$. The last term in Eq. (A.10) is responsible for the elastic anomalies due to iron spin crossover. Using the relation

$$\frac{\partial}{\partial\sigma_i} \equiv \frac{\partial}{\partial P}\frac{\partial P}{\partial\sigma_i} = \frac{1}{3}\frac{\partial}{\partial P}, \tag{A.11}$$

for $i = 1 - 3$ and $\frac{\partial n}{\partial \sigma_4} = \frac{\partial n}{\partial \sigma_5} = \frac{\partial n}{\partial \sigma_6} = 0$ for orthorhombic symmetric system, the elastic compliances are:

$$S^{ij}V = nS^{ij}_{LS}V_{LS} + (1-n)S^{ij}_{HS}V_{HS} - \frac{1}{9}(V_{LS} - V_{HS})\frac{\partial n}{\partial P} \tag{A.12}$$

for $i, j = 1 - 3$ and

$$S^{ii}V = nS^{ii}_{LS}V_{LS} + (1-n)S^{ii}_{HS}V_{HS} \tag{A.13}$$

for $i = 4 - 6$. The elastic constants, C_{ij}, are obtained using the relation: $\mathbf{C}_{ij} = \left[\mathbf{S}^{-1}\right]^{ij}$.

Acknowledgments This work was supported primarily by grants NSF/EAR 1319368, 1348066, and NSF/CAREER 1151738. Computations were performed at the Minnesota Supercomputing Institute (MSI) and at the Blue Waters System at NCSA. Results produced in this study are available in the Supporting Information.

References

References

Alfè, D. (2009), PHON: A program to calculate phonons using the small displacement method, *Comp. Phys. Commun.*, *180*, 26222633, doi:10.1016/j.cpc.2009.03.010.

Andrault, D., N. Bolfan-Casanova, and N. Guignot (2001), Equation of state of lower mantle (Al,Fe)-$MgSiO_3$ pereovskite, *Earth planet. Sci. Lett.*, *193*, 501–508.

Antonangeli, D., J. Siebert, C. M. Aracne, D. L. Farber, A. Bosak, M. Hoesch, M. Krisch, F. J. Ryerson, G. Fiquet, and J. Badro (2011), Spin Crossover in Ferropericlase at High Pressure: A Seismologically Transparent Transition?, *Science*, *331*, 64-67.

Badro J., G. Fiquet, F. Guyot, J. P. Rueff, V. V. Struzhkin, G. Vank, and G. Monaco (2003), Iron Partitioning in Earth's Mantle: Toward a Deep Lower Mantle Discontinuity, *Science*, *300*, 789-791.

Badro J., J. P. R ueff, G. Vanko, G. Monaco, G. Fiquet, and F. Guyot (2004), Electronic Transitions in Perovskite: Possible Nonconvecting Layers in the Lower Mantle, *Science*, *305*, 383.

Baroni, S., A. Dal Corso, S. de Gironcoli, and P. Gianozzi (2001), Phonons and related crystal properties from density-functional perturbation theory, *Rev. Mod. Phys.*, *73(2)*, 515LP–565LP.

Bengtson, A., J. Li, and D. Morgan (2009), Mössbauer modeling to interpret the spin sate of iron in (Mg,Fe)SiO_3, *Geophys. Res. Lett.*, *36*, L15301, doi:10.1029/2009GL038340.

Boehler, R. (2000), High-pressure experiments and the phase diagram of lower mantle and core materials, *Rev. Geophys.*, *38(2)*, 221–245, doi:10.1029/1998RG000053.

Boffa Ballaran, T., A. Kurnosov, K. Glazyrin, D. J. Frost, M. Merlini, M. Hanfland, and R. Caracas (2012), Effect of chemistry on the compressibility of silicate perovskite in the lower mantle, *Earth Planet. Sci. Lett.*, *333-334*, 181–190, doi:10.1016/j.epsl.2012.03.029.

Caracas, R., H. Ishii , M. Hiraoka, Y. Ohishi, and N. Hirao (2014), Identifying the spin transition in Fe^{2+}-rich $MgSiO_3$ perovskite from X-ray diffraction and vibrational spectroscopy , *American Mineralogist*, *99(7)*, 1270–1276, doi:10.2138/am.2014.4783.

Carrier, P., R. M. Wentzcovitch, and J. Tsuchiya (2007), First principles prediction of crystal structures at high temperatures using the quasiharmonic approximation, *Phys. Rev. B*, *76*, 064116, doi:10.1103/PhysRevB.76.064116.

Catalli, K., S.-H. Shim, V. B. Prakapenka, J. Zhao, W. Sturhahn, P Chow, Y. Xiao, H. Liu, H. Cynn, and W.J. Evans (2010a), Spin state of ferric iron in $MgSiO_3$ perovskite and its effect on elastic properties, *Earth Planet. Sci. Lett.* , *289*, 68–75.

Catalli, K., S.-H. Shim, P. Dera, V. B. Prakapenka, J. Zhao, W. Struhahn, P. Chow, Y. Xiao, H. Cynn, and W.J. Evans (2011), Effects of the Fe3+ spin transition on the properties of aluminous perovskiteNew insights for lower-mantle seismic heterogeneities, *Earth Planet. Sci. Lett.* , *310*, 293–302, doi:10.1016/j.epsl.2011.08.018.

Ceperley, D. M., and B. J. Alder (1980), Ground state of the electron gas by a stochastic method, *Phys. Rev. Lett.*, *45*, 566–569.

Chantel, J., D. J. Frost,C. A. McCammon, Z. Jing, and Y. Wang (2012), Acoustic velocities of pure and iron-bearing magnesium silicate perovskite measured to 25 GPa and 1200 K, *Geophys. Res. Lett.*, *39*, L19307, doi:10.1029/2012GL053075, 2012.

Cococcioni, M., and S. de Gironcoli (2005), Linear response approach to the calculation of the effective interaction parameters in the LDA+U method, *Phys. Rev. B*, *71*, 035105.

Crowhurst, J. C., J. M. Brown, A. F. Goncharov, and S. D. Jacobsen (2008), Elasticity of (Mg,Fe)O through the spin transition of iron in the lower mantle, *Science*, *319*, 451–453, doi:10.1126/science.1149606.

da Silva, P., C. R. S. da Silva and R. M. Wentzcovitch (2008), Metadata management for distributed first principles calculations in VLab - A collaborative cyberinfrastructure for materials computation, *Comp. Phys. Comm.*, *178*, 186, doi:10.1016/j.cpc.2007.09.001.

Dorfman, S. M., Y. Meng, V. B. Prakapenka, and T. S. Duffy (2013), Effects of Fe-enrichment on the equation of state and stability of $(Mg,Fe)SiO_3$ perovskite, *Earth Planet. Sci. Lett.*, *361*, 249–257.

Dubrovinsky, L., T. Boffa-Ballaran , K. Glazyrin , A. Kurnosov , D. Frost , M. Merlini , M. Hanfland , V.B. Prakapenka , P. Schouwink , T. Pippinger, and N. Dubrovinskaia (2010), Single-crystal X-ray diffraction at megabar pressures and temperatures of thousands of degrees, *High Pressure Research*, *30(4)*, 620–633.

Dziewonski, A. M., and D. L. Anderson (1981), Preliminary reference Earth model, *Phys. Earth Planet. Int.*, *25*, 297–356.

Fiquet, G., A. Dewaele, D. Andrault, M. Kunz, and T. L. Bihan (2000), Thermoelastic properties and crystal structure of $MgSiO_3$ perovskite at lower mantle pressure and temperature conditions, *Geophys. Res. Lett.*, *27(1)*, 21–24.

Floris, A., S. de Gironcoli, E. K. U. Gross, and M. Cococcioni (2011), Vibrational properties of MnO and NiO from DFT +U-based density functional perturbation theory, *Phys. Rev. B*, *84*, 161102(R).

Fujino, K., D. Nishio-Hamane, Y. Seto, N. Sata, T. Nagai, T. Shinme, T. Irifune, H. Ishii, N. Hiraoka, Y. Q. Cai, K. D. Tsue (2012), Spin transition of ferric iron in Al-bearing Mgperovskite up to 200 GPa and its implication for the lower mantle, *Earth Planet. Sci. Lett.*, *317-318*, 407–412.

Fujino, K., D. Nishio-Hamane, T. Nagai, Y. Seto, Y. Kuwayama, M. Whitaker, H. Ohfuji, T. Shinmei, and T. Irifune (2012), Spin transition, substitution, and partitioning of iron in lower mantle minerals, *Phys. Earth Planet. Inter.*, *228*, 186–191, doi:10.1016/j.pepi.2013.12.008.

Goncharov, A. F., V. V. Struzhkin, and S. D. Jacobsen (2006), Reduced Radiative Conductivity of Low-Spin (Mg,Fe)O in the Lower Mantle, *Science*, *312*, 1205–1208, doi:10.1126/science.1125622.

Himmetoglu, B., A. Floris, S. de Gironcoli, and M. Cococcioni (2014), Hubbard-Corrected DFT Energy Functionals: The LDA+U Description of Correlated Systems, *Int. J. Quantum Chem*, *114*, 14–49, doi:10.1002/qua.24521.

Hsu, H., K. Umemoto, M. Cococcioni, and R. M. Wentzcovitch (2009), First principles study of low-spin LaCoO3 with structurally consistent Hubbard U, *Phys. Rev. B*, *79*, 125124, doi:10.1103/PhysRevB.79.125124.

Hsu, H., K. Umemoto, R. M. Wentzcovitch, and P. Blaha (2010), Spin states and hyperfine interactions of iron in $(Mg,Fe)SiO_3$ perovskite under pressure, *Earth Planet. Sci. Lett.*, *294*, 19–26, doi:10.1016/j.epsl.2010.02.031.

Hsu, H., P. Blaha, M. Cococcioni, and R. M. Wentzcovitch (2011), Spin-state crossover and hyperfine interactions of ferric iron in $MgSiO_3$ perovskite, *Phys. Rev. Lett.*, *106*, 118501, doi:10.1103/PhysRevLett.106.118501.

Hsu, H., Y. Yu, and R. M. Wentzcovitch (2012), Effects of aluminum on spin-state crossover of iron in the Earth's lower mantle, *Earth Planet. Sci. Lett.*, *359-360*, 34–39, doi:10.1016/j.epsl.2012.09.029.

Hsu, H., and R. M. Wentzcovitch (2014), First-principles study of intermediate-spin ferrous iron in the Earth's lower mantle, *Phys. Rev. B*, *90(19)*, 195205, doi:10.1103/PhysRevB.90.195205.

Hummer, D. R., and Y. Fei (2012), Synthesis and crystal chemistry of Fe^{3+}-bearing $(Mg,Fe^{3+})(Si,Fe^{3+})O_3$ perovskite, *American Mineralogist*, *97*, 1915–2012.

Irifune, T., T. Shinmei, C. A. McCammon, N. Miyajima, D. C. Rubie, and D. J. Frost (2010), Iron partitioning and density changes of pyrolite in Earth's lower mantle, *Science*, *327*, 5962, doi:0.1126/science.1181443.

Jackson, J. M., J. Zhang, and J. D. Bass (2004), Sound velocities and elasticiy of al uminous $MgSiO_3$ pervoskite: Implications for aluminum heterogeneity in Earth's lower mantle, *Geophys. Res. Lett.*, *31*, L10614, doi:10.1029/2004GL019918.

Jackson, J.M., W. Sturhahn, G. Shen, J. Zhao, M. Y. Hu, D. Errandonea, J. D. Bass, and Y. Fei (2005a), A synchrotron Mssbauer spectroscopy study of $(Mg,Fe)SiO_3$ perovskite up to 120 GPa, *Am. Mineral.*, *90*, 199–205.

Jackson, J. M., J. Zhang, Shu, S. V. Sinogeikin, and J. D. Bass (2005b), High-pressure sound velocities and elasticity of aluminous $MgSiO_3$ perovskite to 45 GPa: Implications for lateral heterogeneity in Earths lower mantle, *Geophys. Res. Lett.*, *32*, L21305, doi:10.1029/2005GL023522.

Jackson, J. M., S. V. Sinogeikin, S. D. Jacobsen, H. J. Reichmann, S. J. Mackwell, and J. D. Bass (2006), Single-crystal elasticity and sound velocities of $(Mg_{0.94}Fe_{0.06})O$ ferropericlase to 20 GPa, *J. Geophys. Res.*, *111*, B09203, doi:10.1029/2005JB004052.

Karki, B. B., R. M. Wentzcovitch, S. de Gironcoli, and S. Baroni (1999), First principles determination elastic anisotropy and wave velocities of MgO at lower mantle conditions, *Science*, *286*, 1705.

Karki, B. B., R. M. Wentzcovitch, S. de Gironcoli, and S. Baroni (2001), First principles thermoelasticity of $MgSiO_3$-perovskite: consequences for the inferred properties of the lower mantle, *Geophys. Res. Lett.*, *28*, 2699–2702.

Kiefer, B., L. Stixrude, and R. M. Wentzcovitch (2002), Elasticity of $(Mg,Fe)SiO_3$-perovskite at lower mantle conditions, *Geophys. Res. Lett.*, *29*, 1–4.

Kulik, H., M. Cococcioni, D. A. Scherlis, and N. Marzari (2006), Density functional theory in transition metal chemistry: a self-consistent Hubbard U approach, *Phys. Rev. Lett.*, *97*, 103001.

Kupenko, I., C. McCammon, R. Sinmyo, C. Prescher, A. I. Chumakov, A. Kantor,R. R*ü*ffer, and D. Dubrovinsky(2014), Electronic spin state of Fe,Al-containing $MgSiO_3$ perovskite at lower mantle conditions , *Lithos*, *189*, 167–172 doi:10.1016/j.lithos.2013.10.022.

Leiria Campo Jr., V., and M. Cococcioni (2010), Extended DFT + U + V method with on-site and inter-site electronic interactions, *J. Phys.: Condens. Matter*, *22*, 055602, doi:10.1088/0953-8984/22/5/055602.

Li, B., and J. Zhang, (2005), Pressure and temperature dependence of elastic wave velocity of MgSiO3 perovskite and the composition of the lower mantle, *Phys. Earth Planet. Inter.*, *151*, 143–154, doi:10.1016/j.pepi.2005.02.004.

Li, J., V. V. Struzhkin, H. K. Mao, J. Shu, R. J. Hemley, Y. Fei, B. Mysen, P. Dera, V. Prakapenka, and G. Shen (2004), Electronic spin state of iron in lower mantle perovskite, *Proc. Natl. Acad. Sci.*, *101*, 14027–14030.

Li, J., W. Sturhahn, J. M. Jackson, V. V. Struzhkin, J. F. Lin, J. Zhao, H. K. Mao, and G. Shen (2006), Pressure effect on the electronic structure of iron in (Mg,Fe)(Si,Al)O_3 perovskite: A combined synchrotron Mssbauer and X-ray emission spectroscopy study up to 100 GPa, *Phys. Chem. Minerals*, *33*, 575–585.

Lin, J., H. Watson, G. Vanko, E. E. Alp, V. B. Prakapenka, P. Dera, V. V. Struzhkin, A. Kubo, J. Zhao, C. McCammon, and W. J. Evans (2008), Intermediate-spin ferrous iron in lowermost mantle post-perovskite and perovskite, *Natl. Geosci*, *1*, 688–691.

Lin, J. F., E. E. Alp, Z. Mao, T. Inoue, C. McCammon, Y. Xiao, P. Chow, and J. Zhao (2012), Electronic spin and valence states of iron in the lower-mantle silicate perovskite by synchrotron Mssbauer spectroscopy, *American Mineralogist*, *97*, 592–597.

Lin, J. F., S. Speziale, Z. Mao, and H. Marquardt (2013), Effects of the electronic spin transitions of iron in lower-mantle minerals: implications to deep-mantle geophysics and geochemistry, *Rev. Geophys.*, *51*, 244–275.

Lundin, S., L. Catalli, J. Santillan, S.-H. Shim, V. B. Prakapenka, M. Kunz, and Y. Meng (2008), Effect of Fe on the equation of state of mantle silicate perovskite over 1 Mbar, *Phys. Earth Planet. Inter.*, *168*, 97–102.

Mao, Z., J.-F. Lin, J. Yang, T. Inoue, and V. B. Prakapenka (2015), Effects of the Fe^{3+} spin transition on the equation of state of bridgmanite, *Geophys. Res.Lett.*, *42*, 4335–4342.

Marquardt M., S. Speziale, H. J. Reichmann, D. J. Frost, F. R. Schilling, and E. J. Garnero (2009), Elastic Shear Anisotropy of Ferropericlase in Earth's Lower Mantle, *Science*, *324*, 224–226, doi:10.1126/science.1169365.

McCammon, C., I. Kantor, O. Narygina, J. Rouquette, U. Ponkratz, I. Sergueev, M. Mezouar, V. Prakapenka, and L. Dubrovinsky (2008), Stable intermediate-spin ferrous iron in lower-mantle perovskite, *Nat. Geosci.*, *1*, 684–687.

McCammon, C., K. Glazyrin, A. Kantor, I. Kantor, I. Kupenko, O. Narygina, V. Potapkin, C. Prescher, R. Sinmyo, A. Chumakov, R. Rüffer, I. Sergueev, G. Smirnov, and L. Dubrovinsky (2013), Iron spin state in silicate perovskite at conditions of the Earth's deep interior, *High Press. Res.*, *43(3)*, 663–672.

Monkhorst, H. J., and J. D. Pack (1976), Special points for Brillouin-zone integrations, *Phys. Rev. B*, *13*, 5188–5192.

Murakami, M., S. V. Sinogeikin, H. Hellwig, J. D. Bass, and J. Li (2007), Sound velocity of $MgSiO_3$ perovskite to Mbar pressure, *Earth Planet. Sci. Lett.*, *256*, 47–54, doi:10.1016/j.epsl.2007.01.011.

Murakami, M., Y. Ohishi, N. Hirao, and K. Hirose (2012), A perovskitic lower mantle inferred from high-pressure, high-temperature sound velocity data, *Nature*, *485*, 90–94, doi:10.1038/nature11004.

Oganov, A. R., J. P. Brodholt, and G. D. Price (2001a), Ab initio elasticity and thermal equation of state of $MgSiO_3$ perovskite, *Earth Planet. Sci. Lett.*, *184*, 555–560.

Oganov, A. R., J. P. Brodholt, and G. D. Price (2001b), The elastic constants of $MgSiO_3$ perovskite at pressure and temperatures of the Earth's mantle , *Nature*, *411*, 934–9370 doi:10.1038/35082048.

Potapkin, V, C. McCammon, K. Glazyrin, A. Kantor, I. Kupenko, C. Prescher, R. Sinmyo, G. V. Smirnov, A. I. Chumakov, R. Rüffer, and L. Dubrovinsky (2013), Effect of iron oxidation state on the electrical conductivity of the Earth's lower mantle , *Nature Communication*, *4*,1427.

Sinnelnikov, Y. D., G. Chen, D. R. Neuville, M. T. Vaughan, and R. C. Liebermann (1998), Ultrasonic shear wave velocities of $MgSiO_3$ perovskite at 8 GPa and 800 K and lower mantle composition, *Science* , *281*, 667–679.

Shukla, G., Z. Wu, H. Hsu, A. Floris, M. Cococcioni, and R. M. Wentzcovitch (2015), Thermoelasticity of Fe^{2+}-bearing bridgmanite, *Geophys. Res. Lett.*, *42*, 1741-1749.

Shukla, G., M. Topsakal, and R. M. Wentzcovitch (2015), Spin crossovers in iron-bearing $MgSiO_3$ and $MgGeO_3$: Their influence on the post-perovskite transition, *Phys. Earth Planet. Inter.*, *249*, 11–17.

Sinmyo R., E. Bykova, C. McCammon, I Kupenko, VPotapkin , and L. Dubrovinsky (2014), Crystal chemistry of Fe^{2+}bearing (Mg,Fe)SiO3 perovskite: a singlecrystal Xray diffraction study, *Phys. Chem. Minerals*, *41*, 409-417.

Sinogeikin, S. V., J. Zhang, and J. D. Bass (2004), Elasticity of single crystal and polycrystalline $MgSiO_3$ perovskite by Brillouin spectroscopy, *Geophys. Res. Lett.*, *31*, L06620, doi:10.1029/2004GL019559.

Stackhouse, S., J. P. Brodholt, and G. D. Price (2007), Electronic spin transitions in iron-bearing $MgSiO_3$ perovskite, *Earth Planet. Sci. Lett.*, *253*, 282–290.

Tsuchiya, T., R. M. Wentzcovitch, C. R. S. da Silva, S. de Gironcoli (2006), Spin transition in magnesiowstite in Earth's lower mantle, *Phys. Rev. Lett.*, *96(19)*, 198501.

Tsuchiya, T., and X. Wang (2013), Ab initio investigation on the high-temperature thermodynamic properties of Fe^{3+}-bearing $MgSiO_3$ perovskite, *J. Geophys. Res. Solid Earth*, *118*, 83–91.

Umemoto, K., R. M. Wentzcovitch, Y. Yu, and R. Requist (2008), Spin transition in (Mg,Fe)SiO_3 perovskite under pressure, *Earth Planet. Sci. Lett.*, *276*, 198–206, doi:10.1016/j.epsl.2008.09.025.

Vanderbilt, D., (1990), Soft self-consitent pseudopotentials in a genrelized eigenvalue formalism, *Phys. Rev. B*, *41*, 7892–7895.

Wallace, D. C., (1972), Thermodynamic of Crystals, John Wiley & Sons, Inc., USA.

Wang, X.L., T. Tsuchiya, and A. Hase (2015), Computational support for a pyrolitic lower mantle containing ferric iron, *Nat. Geosci.*, *8*, 556–559.

Watt, J. P., G. F. Davies, and R. J. OConnell (1976), The elastic properties of composite materials, *Rev. Geophys. Space Phys.*, *50*, 6290–6295.

Wentzcovitch, R. M., (1991), Invariant molecular dynamics approach to structural phase transitions, *Phys. Rev. B*, *44*, 2358-2361.

Wentzcovitch, R. M., J. L. Martins, and G. D. Price (1993), Ab initio molecular dynamics with variable cell shape: application to $MgSiO_3$, *Phys. Rev. Lett.*, *70*, 3947.

Wentzcovitch, R. M., B. B. Karki, M. Cococcioni, and S. de Gironcoli (2004), Thermoelastic properties of of $MgSiO_3$-perovskite: insights on the nature of the Earths lower mantle, *Phys. Rev. Lett.*, *92*, 018501.

Wentzcovitch, R. M., J. F. Justo, Z. Wu, C. R. S da Silva, A. Yuen, and D. Kohlstedtd (2009), Anomalous compressibility of ferropericlase throughout the iron spin cross-over, *Proc. Natl. Acad. Sci.* , *106*, 21.

Wentzcovitch, R. M., Y. Yu, and Z. Wu (2010a), Thermodynamic properties and phase relations in mantle minerals investigated by first priniciples quasiharmonic theory,*Reviews in Mineralogy and Geochemistry*, *71*, 59–98.

Wentzcovitch, R. M., Z. Wun and P Carrie (2010b), First priniciples quasiharmonic thermoelasticity of mantle minerals, *Reviews in Mineralogy and Geochemistry*,*71*, 99–128.

Wu, Z., J. F. Justo, C. R. S. da Silva, S. de Gironcoli, and R. M. Wentzcovitch (2009), Anomalous thermodynamic properties in ferropericlase throughout its spin crossover, *Phys. Rev. B*, *80*, 014409.

Wu, Z., and R. M. Wentzcovitch (2011), Quasiharmonic thermal elasticity of crystals: An analytical approach, *Phys. Rev. B*, *83*, 184115.

Wu, Z., J. F. Justo, and R. M. Wentzcovitch (2013), Elastic Anomalies in a Spin-Crossover System: Ferropericlase at Lower Mantle Conditions, *Phys. Rev. Lett.*, *110*, 228501.

Wu, Z., and R. M. Wentzcovitch (2014), Spin crossover in ferropericlase and velocity heterogeneities in the lower mantle, *Proc. Natl. Acad. Sci.*, *111(29)*, 10468–10472.

Xu S., S-H. Shim, and D. Morgan (2015), Origin of Fe^{3+} in Fe-containing, Al-free mantle silicate perovskite, *Earth Planet. Sci. Lett.*, *409*, 319-328.

Zhang, L., Y. Meng, W. Yang, L. Wang, W. L. Mao, Q-S. Zeng, J. S. Jeong, A. J. Wagner, K. A. Mkhoyan, W. Liu, R. Xu, and H-K. Mao, (2014), Disproportionation of (Mg,Fe)SiO_3 perovskite in Earths deep lower mantle, *Science*, *344*, 877.

Zhang, S., S. Cottaar, T. Liu, S. Stackhouse, and B. Militzer (2016), High-pressure, temperature elasticity of Fe- and Al-bearing $MgSiO_3$: Implications for the Earth's lower mantle, *Earth Planet. Sci. Lett.*, *434*, 264–273, doi:10.1016/j.epsl.2015.11.030.

Zhang, Z., L. Stixrude, J. Brodholt (2013), Elastic properties of $MgSiO_3$-perovskite under lower mantle conditions and the composition of the deep Earth, *Earth. Planet. Sci. Lett.*, *379*, 1–12.